

## Localized surface plasmon assisted contrast microscopy for ultrathin transparent specimens

Feifei Wei, Dylan Lu, Ryan Aguinaldo, Yicong Ma, Sunil K. Sinha, and Zhaowei Liu

Citation: [Applied Physics Letters](#) **105**, 163102 (2014); doi: 10.1063/1.4898675

View online: <http://dx.doi.org/10.1063/1.4898675>

View Table of Contents: <http://scitation.aip.org/content/aip/journal/apl/105/16?ver=pdfcov>

Published by the [AIP Publishing](#)

---

### Articles you may be interested in

[A localized surface plasmon resonance-based optical fiber sensor with sub-wavelength apertures](#)

Appl. Phys. Lett. **103**, 193116 (2013); 10.1063/1.4829530

[Transmission surface plasmon resonance microscopy](#)

Appl. Phys. Lett. **103**, 133110 (2013); 10.1063/1.4822431

[Surface enhanced Raman scattering and localized surface plasmon resonance of nanoscale ultrathin films prepared by atomic layer deposition](#)

Appl. Phys. Lett. **101**, 023112 (2012); 10.1063/1.4729411

[Systematic investigation of localized surface plasmon resonance of long-range ordered Au nanodisk arrays](#)

J. Appl. Phys. **103**, 014308 (2008); 10.1063/1.2828146

[Optical fiber affinity biosensor based on localized surface plasmon resonance](#)

Appl. Phys. Lett. **85**, 4231 (2004); 10.1063/1.1812583

---

The advertisement features a dark blue background with a film strip graphic on the left. The text is in white and orange. The main headline reads 'Not all AFMs are created equal' in orange, followed by 'Asylum Research Cypher™ AFMs' in white, and 'There's no other AFM like Cypher' in orange. Below this is the website 'www.AsylumResearch.com/NoOtherAFMLikeIt' in white. In the bottom right corner is the Oxford Instruments logo, which consists of the word 'OXFORD' in a large font above 'INSTRUMENTS' in a smaller font, all within a white rectangular border. Below the logo is the tagline 'The Business of Science®' in a small white font.

## Localized surface plasmon assisted contrast microscopy for ultrathin transparent specimens

Feifei Wei,<sup>1</sup> Dylan Lu,<sup>1</sup> Ryan Aguinaldo,<sup>1</sup> Yicong Ma,<sup>2</sup> Sunil K. Sinha,<sup>2</sup> and Zhaowei Liu<sup>1,3,4,a)</sup>

<sup>1</sup>*Department of Electrical and Computer Engineering, University of California, San Diego, 9500 Gilman Drive, La Jolla, California 92093-0407, USA*

<sup>2</sup>*Department of Physics, University of California, San Diego, 9500 Gilman Drive, La Jolla, California 92093, USA*

<sup>3</sup>*Materials Science and Engineering Program, University of California, San Diego, 9500 Gilman Drive, La Jolla, California 92093, USA*

<sup>4</sup>*Center for Magnetic Recording Research, University of California, San Diego, 9500 Gilman Drive, La Jolla, California 92093-0401, USA*

(Received 8 July 2014; accepted 6 October 2014; published online 20 October 2014)

We demonstrate a high contrast imaging technique, termed localized surface plasmon assisted contrast microscopy, by combining localized surface plasmon resonances (LSPR) and dark-field microscopy technique. Due to the sensitive response of LSPR to the refractive index of the surrounding media, this technique is capable of converting a small refractive index difference to a change in scattering intensity, resulting in a high-contrast, diffraction limited image of a thin unstained specimen with small, gradual refractive-index variation. © 2014 AIP Publishing LLC.

[<http://dx.doi.org/10.1063/1.4898675>]

Optical microscopy is an important tool for life science because light is a non-invasive probe to examine biological samples. Since the refractive indices of cells and subcellular components are very close to water, they normally show small intensity variation under a conventional bright field microscope. Several techniques, such as dark field microscopy and phase contrast microscopy, were invented to enhance the image contrast without staining the biological samples. The dark field microscopy relies on the scattering of the illumination light introduced by the refractive index variation in a sample to form a high contrast image.<sup>1</sup> Whereas, the phase contrast microscopy converts the optical path length difference between the specimen and its surrounding media into the intensity variation in the image by utilizing a condenser annulus combined with a matching phase plate located inside an objective.<sup>1</sup> Although these techniques can greatly improve the image contrast, they all have corresponding limitations. For example, the contrast in dark field microscopy vanishes for specimens with gradual refractive index variation; whereas the image formed by a phase contrast microscope usually shows a characteristic halo and shade-off artifacts.<sup>1</sup>

Besides the aforementioned conventional high contrast microscopy techniques, propagating surface plasmon (SP) or localized SP assisted contrast enhancement techniques were also explored during past few decades.<sup>4–18</sup> SP is the collective oscillation of electrons propagating on metal surface (propagating SP) or confined to metallic-nanostructures (localized SP). Since the excitation conditions for both propagating and localized SP resonances are very sensitive to the local refractive index variation,<sup>2,3</sup> they are widely used in label-free bio-sensing<sup>4–6</sup> and bio-imaging.<sup>7–18</sup> In the field of microscopy, a propagating SP assisted microscopy technique

was first demonstrated in late 1980s and greatly improved the image contrast for thin-film samples with non-uniform refractive index.<sup>7,8</sup> However, its spatial resolution is limited by the propagation length of SPs and is on the order of microns.<sup>7,8</sup> To improve the spatial resolution, microscope objectives were then used to excite propagating SP and several scanning or wide field approaches have been demonstrated.<sup>9–15</sup> The scanning approaches<sup>9–11</sup> achieve relatively higher spatial resolution (~200–300 nm), but sacrifice the image acquisition time compared with the wide field techniques.<sup>12–15</sup>

Compared with the propagating SP assisted microscopy techniques, localized SP assisted imaging techniques intrinsically possess high spatial resolution, because the localized SP field is confined within tens to hundreds of nanometers region around the deep sub-diffraction-limited nanostructures and only the local refractive indices influence the LSPR characteristics.<sup>5</sup> Moreover, the LSPR can be observed using a standard dark field microscope with no additional modification to the optics, which makes the system easy to implement and ready to use. Therefore, metallic-nanostructures directly patterned on a substrate have become widely used for refractive index sensing.<sup>5,18</sup> However, utilizing such patterned substrates to enhance the image contrast of thin specimens with small, gradual refractive index variations have not been demonstrated yet.

In this Letter, we demonstrate a localized SP assisted contrast (LSPAC) microscopy technique by combining LSPR of the metallic-nanostructure patterned substrate and dark field microscopy. The thin specimen is placed on top of the patterned substrate and the scattered light is collected by standard dark field microscopy, as is shown by the schematic configuration in Fig. 1(a). Owing to the sensitive response of the LSPR peak wavelength with respect to the refractive index of the surrounding media, the LSPR peak wavelength

<sup>a)</sup> Author to whom correspondence should be addressed. Electronic mail: zhaowei@ece.ucsd.edu

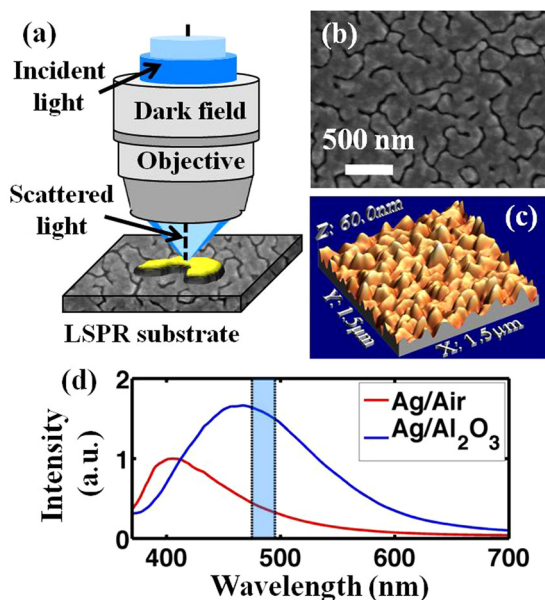


FIG. 1. (a) Schematic configuration of the LSPAC microscopy system; (b) SEM image, (c) AFM image, and (d) the scattering spectra of the porous Ag film. The spectrum is normalized with respect to the illumination spectrum. The shaded blue region in (d) corresponds to the wavelength range of the illumination light used for the microscopy measurement.

of the metallic-nanostructure patterned substrate shifts with the local refractive index variation of the thin specimen placed on top. Therefore, the corresponding scattering image of the thin specimen shows different colors at different refractive index regions. By applying a bandpass illumination filter, this LSPR peak wavelength shift is then converted to the scattering intensity difference, which eventually leads to the image contrast enhancement. Since the LSPR peak wavelength is more sensitive to the refractive index of the material that is closer to the nanostructures, due to the strong field confinement, the thickness of the sample should be comparable to or smaller than the penetration depth of the localized SP field, which is normally around tens to hundreds of nanometers.<sup>5,19</sup>

In principle, the substrate for LSPAC microscopy can be any kind of metallic-nanostructure patterned substrate that supports appropriate LSPR. Here, we choose a porous silver (Ag) film due to its strong scattering signal and easy fabrication process for a proof-of-concept demonstration. A layer of 60 nm thick porous Ag film was deposited on a cover slip by electron beam deposition at a deposition rate of 0.7 Å/s with a base pressure of  $2 \times 10^{-7}$  Torr. During the deposition, Ag first forms sparse islands and then individual islands gradually merge together to form a continuous film as the film thickness increases.<sup>20</sup> However, the slow deposition rate and small film thickness used for our substrate fabrication result in lots of random distributed air gaps in the film as indicated by both the scanning electron microscope (SEM) and atomic force microscope (AFM) images in Figs. 1(b) and 1(c), respectively. In addition to the surface metrology characterization, the scattering response of the deposited porous Ag film was also collected by a Zeiss 50× objective (LD EC Epiplan-Neofluar), and then analyzed by a spectrometer. The red and blue curves in Fig. 1(d) correspond to the scattering spectra of the porous Ag film with a surrounding overlayer

of air ( $n = 1.0$ ) and  $\text{Al}_2\text{O}_3$  ( $n = 1.74$ ), respectively. As the refractive index of the surrounding medium increases, the LSPR peak wavelength shifts from  $\sim 405$  nm to  $\sim 467$  nm.

To demonstrate the high contrast imaging capability of LSPAC microscopy, an array of thin  $\text{Al}_2\text{O}_3$  squares was deposited on top of both the porous Ag substrate and a bare cover slip, serving as the LSPAC sample and the control sample, respectively. The  $40 \mu\text{m}$  wide and  $\sim 40$  nm thick  $\text{Al}_2\text{O}_3$  squares were fabricated by electron beam deposition with a gold grid as the shadow mask. Based on the spectra of the porous Ag substrate, an illumination wavelength close to the LSPR peak at the  $\text{Al}_2\text{O}_3/\text{Ag}$  interfaces ( $485 \text{ nm} \pm 10 \text{ nm}$ , indicated by the blue region in Fig. 1(d)) was selected for the LSPAC sample and control sample microscopy measurements. For the  $\text{Al}_2\text{O}_3$  squares deposited on the porous Ag substrate, stronger scattering signals are collected at the  $\text{Al}_2\text{O}_3/\text{Ag}$  region as shown in Fig. 2(a) compared to that collected at the Air/Ag region. This is due to the red shift of the LSPR peak wavelength introduced by the refractive index difference between air ( $n = 1.0$ ) and  $\text{Al}_2\text{O}_3$  ( $n = 1.74$ ). The contrast between the bright  $\text{Al}_2\text{O}_3$  squares and the dark surrounding air region is about 60% (calculated by  $\frac{I_{\text{max}} - I_{\text{min}}}{I_{\text{max}} + I_{\text{min}}}$ ), which matches the contrast calculated from the scattering spectra of the  $\text{Al}_2\text{O}_3/\text{Ag}$  and Air/Ag (Fig. 1(d)) at  $485 \text{ nm} \pm 10 \text{ nm}$ . As for the phase contrast microscopy image of the control sample, the intensity contrast is limited, as shown in Fig. 2(b), due to the small optical path length difference between the air and the deposited  $\text{Al}_2\text{O}_3$  squares. The reflection bright field image of the control sample shows a weak contrast (Fig. 2(c)) because of the reflectivity differences between the air and the  $\text{Al}_2\text{O}_3$  squares on the cover slip. Moreover, only the edges that correspond to refractive index discontinuity regions scatter light and form the outline of the  $\text{Al}_2\text{O}_3$  squares (Fig. 2(d)) in the reflection dark field image of the control sample.

As a further demonstration of the contrast enhancement capability of the LSPAC, an  $\text{Al}_2\text{O}_3$  taper was selected as the testing object with a gradual average-refractive-index

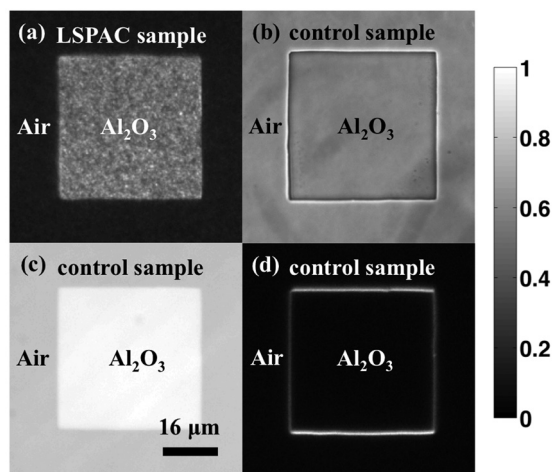


FIG. 2. (a) The scattering image of the  $\text{Al}_2\text{O}_3$  squares deposited on the porous Ag film (the LSPAC sample); (b) the phase contrast image; (c) the reflection bright field image; and (d) the reflection dark field image of the  $\text{Al}_2\text{O}_3$  squares deposited on a cover slip (the control sample). (a), (c), and (d) Taken with the same 50× objective used for Fig. 1(d); and (b) taken with a Zeiss 100× phase contrast objective (Plan-Apochromat Ph3).

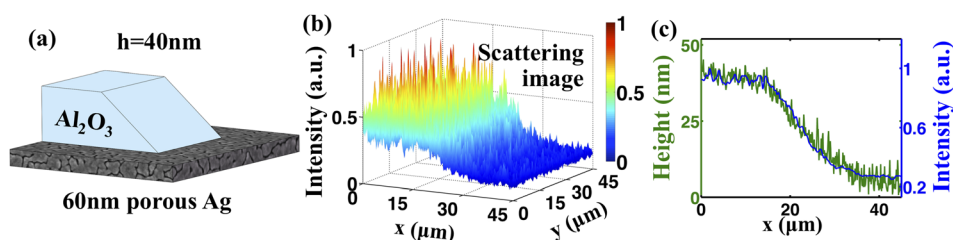


FIG. 3. (a) Schematics of the  $\text{Al}_2\text{O}_3$  taper deposited on the porous Ag film. (b) The scattering image, (c) its cross section (blue line), and the AFM measurement (green line) of the  $\text{Al}_2\text{O}_3$  taper deposited on the porous Ag film. (b) Taken with the same  $50\times$  objective used for Fig. 1(d).

variation, due to its simple fabrication process. For a LSPR substrate, if the thin sample placed on top contains multiple materials along the normal direction, the refractive index of each material influences the LSPR peak wavelength, which means that the LSPR substrate responds to the average-refractive-index within its localized SP field range. The  $\text{Al}_2\text{O}_3$  taper was deposited on both the porous Ag substrate and a bare cover slip substrate by electron beam deposition using another cover slip as a shadow mask. The shadow mask is placed 1 mm above the top of the substrates so that the thickness of the deposited  $\text{Al}_2\text{O}_3$  films gradually decreases from  $\sim 40$  nm to 0 nm within about a  $20\ \mu\text{m}$  region as shown by both the schematic drawing (Fig. 3(a)) and the AFM measurement (Fig. 3(c), green line). Therefore, the average-refractive-index of a 40 nm thick layer at the taper region linearly decreases from 1.74 to 1.00, accordingly. For the  $\text{Al}_2\text{O}_3$  taper deposited on the porous Ag substrate, the gradual decrease of the average-refractive-index causes the LSPR peak wavelength to gradually shift toward shorter wavelengths. Therefore, different scattered light intensity is collected at different locations in the taper region with a narrow band illumination light. Figure 3(b) shows the normalized scattering intensity distribution at the taper region with both the height and color representing the scattering intensity under  $485\ \text{nm} \pm 10\ \text{nm}$  illumination. Since the passing band of the filter is close to the LSPR peak for  $\text{Al}_2\text{O}_3/\text{Ag}$  interface, the scattering intensity is strongest at the uniform 40 nm  $\text{Al}_2\text{O}_3$  region, and then gradually decreases at the taper area as the  $\text{Al}_2\text{O}_3$  thickness decreases, and finally stabilizes at the air region. If the taper region is treated as one object with fixed height and varying refractive index, the scattering intensity can be related to the local refractive index variation of the object. However, if the taper region is considered as an object with fixed refractive index but varying height, the scattering intensity reveals the height variation of the taper, as confirmed by the agreement of averaged scattering intensity at the taper region (Fig. 3(c), blue line) and the AFM height measurement of  $\text{Al}_2\text{O}_3$  taper (Fig. 3(c), green line). For the taper deposited on the cover slip, the scattered light is extremely weak due to the slow variation of the average-refractive-index with respect to the spatial location. As a result, the taper is not visible under conventional reflection dark field microscopy. Moreover, the conventional phase contrast microscopy also fails to provide contrast enhancement due to the small optical path length variation between the deposited  $\text{Al}_2\text{O}_3$  and air.

To demonstrate the bio-imaging capability of the LSPAC microscopy, a multilayer lipid film was deposited onto a porous Ag substrate. The lipid film consists of DOPC (1,2-Dioleoyl-sn-glycero-3-phosphocholine) molecules, which were originally dissolved in 1:1 chloroform and TFE

(2,2,2-Trifluoroethanol) solution. After being spin coated onto both the porous Ag substrate and a bare cover slip, the solvent evaporates and multilayer lipid film forms on the substrates through self-assembling process. The scattering image of the LSPAC sample, shown in Figs. 4(a) and 4(c), was acquired under  $485\ \text{nm} \pm 10\ \text{nm}$  illumination and shows about 50% contrast between the bright and dark regions. Compared with the reflection bright field image of the lipid film on the cover slip (Fig. 4(b), top), the image contrast is significantly enhanced; whereas the reflection dark field image in Fig. 4(b) bottom only show the edges. As discussed in the previous session, the purpose of the bandpass filter is to convert the LSPR wavelength shift introduced by either the refractive or the film thickness changes within the near field of the LSPR substrate to scattering intensity differences. Because the refractive index of the lipid film is constant, the scattering intensity change corresponds to the lipid film thickness variation, as confirmed by the comparison between the magnified scattering image (Fig. 4(c)) and the AFM measurement (Fig. 4(d)) within the white dashed square in Fig. 4(a).

Since the high contrast imaging capability of the LSPAC microscopy comes from the LSPR peak shift with the refractive index variation in the surrounding media, the imaging contrast is mainly determined by the substrate sensitivity and the full width half maximum (FWHM) of its

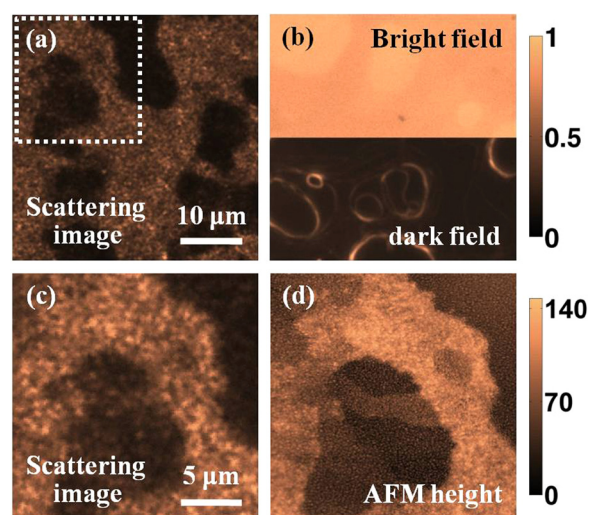


FIG. 4. (a) The scattering image of a multilayer lipid film deposited on the porous Ag substrate. (b) The reflection bright field (top) and dark field images (bottom) of a multilayer lipid film deposited on a cover slip. (c) The magnified scattering image and (d) the AFM height measurement of the white dashed square region in (a). (a)–(c) Taken with the same  $50\times$  objective used for Fig. 1(d) and normalized to their max intensity. The colorbar for the AFM height in (d) is in nm. The imaging areas for Figs. 4(b) and 4(d) are the same as Figs. 4(a) and 4(c), respectively.

resonance peak. A LSPR substrate with higher sensitivity and narrower resonance peak can provide better contrast enhancement. The porous Ag substrate used in this paper is for proof-of-concept demonstration purpose. Depending on the specific requirement of the object, other plasmonic materials, such as Au or Al, could be used for the substrate fabrication. The porous Ag substrate contains sub-diffraction-limited LSPR structures, whose sizes are controllable by the deposition condition,<sup>20</sup> and is easy to fabricate with low cost. To further improve the contrast enhancement factor, specially designed nanostructures that have sharp resonance peak or high sensitivity,<sup>21–24</sup> such as triangular nanoprisms, could be used as the LSPR substrates. During the image acquisition, the LSPR peak wavelength shift is converted to the intensity variation by illumination filters. Therefore, the image contrast is also influenced by the center wavelength and the bandwidth of the bandpass filters. Using filters with appropriate center wavelength and narrower bandwidth can result in higher contrast enhancement for the same sample. Besides sensitivity, lateral spatial resolution is also an important factor for an imaging system. The spatial resolution of LSPAC microscopy is only limited by the diffraction limit of the microscope to  $\sim 0.61 \lambda/\text{NA}$  (about 300–600 nm for visible light), in which  $\lambda$  is the detection wavelength and NA is the numerical aperture of the objective. Moreover, because of the z direction field confinement, the LSPAC microscopy is less sensitive to the refractive index change far from the substrate and is excellent for enhancing the imaging contrast of thin samples. Finally, the non-uniform scattering intensity in uniform  $\text{Al}_2\text{O}_3$  or air region is caused by the non-uniformity of porous Ag substrate and can be significantly reduced by better substrate designs and fabrication techniques.

In conclusion, our experimental results show that by replacing conventional cover slips with metallic-nanostructure patterned substrates, LSPAC microscopy is capable of acquiring wide field, high contrast images of thin specimens with small, gradual refractive index variations. Since its high contrast imaging capability originates from localized SP instead of propagating SP, its spatial resolution is only limited by the diffraction limit of the imaging objective, about several hundred nanometers. Moreover, this technique is a wide field technique, and thus no scanning or additional modification of the optical path is needed for the image acquisition, which makes the system easy to implement and use. Finally, the LSPR substrate can be further

integrated with other Lab-on-a-chip structures, such as micro-fluid channels, to accomplish high contrast imaging on a multi-function chip and may have potential applications in fields such as bio-imaging, sensing, and point-of-care diagnostics.

This work was partially supported by the NSF-ECCS under Grant No. 0969405. Yicong Ma's work was supported by Office of Basic Energy Sciences DOE, under Grant No. DE-FG02-04ER46173.

- <sup>1</sup>D. B. Murphy, *Fundamentals of Light Microscopy and Electronic Imaging* (Wiley-Liss, Inc., 2001).
- <sup>2</sup>H. Raether, *Surface Plasmons on Smooth and Rough Surfaces and on Gratings* (Springer-Verlag: Berlin Heidelberg, Germany, 1988).
- <sup>3</sup>S. A. Maier, *Plasmonics: Fundamentals and Applications* (Springer, 2007).
- <sup>4</sup>J. Homola, *Anal. Bioanal. Chem.* **377**, 528–539 (2003).
- <sup>5</sup>K. A. Willets and R. P. Van Duyne, *Annu. Rev. Phys. Chem.* **58**, 267–297 (2007).
- <sup>6</sup>P. L. Stiles, J. A. Dieringer, N. C. Shah, and R. P. Van Duyne, *Annu. Rev. Anal. Chem.* **1**, 601–626 (2008).
- <sup>7</sup>B. Rothenhausler and W. Knoll, *Nature* **332**, 615–617 (1988).
- <sup>8</sup>W. Hickel, D. Kamp, and W. Knoll, *Nature* **339**, 186 (1989).
- <sup>9</sup>M. G. Somekh, S. G. Liu, T. S. Velinov, and C. W. See, *Opt. Lett.* **25**(11), 823–825 (2000).
- <sup>10</sup>K. Watanabe, N. Horiguchi, and H. Kano, *Appl. Opt.* **46**(22), 4985–4990 (2007).
- <sup>11</sup>K. Watanabe, M. Ryosuke, G. Terakado, T. Okazaki, K. Morigaki, and H. Kano, *Appl. Opt.* **49**(5), 887–891 (2010).
- <sup>12</sup>G. Stabler, M. G. Somekh, and C. W. See, *J. Microsc.* **214**(3), 328–333 (2004).
- <sup>13</sup>M. Mahadi Abdul Jamil, M. Youseffi, P. C. Twigg, S. T. Britland, S. Liu, C. W. See, J. Zhang, M. G. Somekh, and M. C. T. Denyer, *Sens. Actuators, B* **129**, 566–574 (2008).
- <sup>14</sup>R. Vander and S. G. Lipson, *Opt. Lett.* **34**(1), 37–39 (2009).
- <sup>15</sup>M. G. Somekh, G. Stabler, S. Liu, J. Zhang, and C. W. See, *Opt. Lett.* **34**(20), 3110–3112 (2009).
- <sup>16</sup>A. C. Curry, M. Crow, and A. Wax, *J. Biomed. Opt.* **13**(1), 014022 (2008).
- <sup>17</sup>J. Aaron, K. Travis, N. Harrison, and K. Sokolov, *Nano Lett.* **9**(10), 3612–3618 (2009).
- <sup>18</sup>M. P. Raphael, J. A. Christodoulides, S. P. Mulvaney, M. M. Miller, J. P. Long, and J. M. Byers, *Anal. Chem.* **84**, 1367–1373 (2012).
- <sup>19</sup>L. Chen, H. Wei, K. Q. Chen, and H. X. Xu, *Chin. Phys. B* **23**(2), 027303 (2014).
- <sup>20</sup>R. S. Sennett and G. D. Scott, *J. Opt. Soc. Am.* **40**(4), 203–211 (1950).
- <sup>21</sup>L. J. Sherry, S. H. Chang, G. C. Schatz, and R. P. Van Duyne, *Nano Lett.* **5**(10), 2034–2038 (2005).
- <sup>22</sup>L. J. Sherry, R. Jin, C. A. Mirkin, G. C. Schatz, and R. P. Van Duyne, *Nano Lett.* **6**(9), 2060–2065 (2006).
- <sup>23</sup>K. Munechika, J. M. Smith, Y. Chen, and D. S. Ginger, *J. Phys. Chem. C* **111**(51), 18906–18911 (2007).
- <sup>24</sup>L. B. Sagle, L. K. Ruvuna, J. A. Ruellemele, and R. P. Van Duyen, *Nanomedicine* **6**(8), 1447–1462 (2011).